Biosensors and Bioelectronics 133 (2019) 169–176

Contents lists available at ScienceDirect

Biosensors and Bioelectronics

journal homepage: www.elsevier.com/locate/bios

Integrated microfluidic pneumatic circuit for point-of-care molecular diagnostics

Suyeon Shin, Byeongyeon Kim, Yoon-Jin Kim*, Sungyoung Choi*

Department of Biomedical Engineering, Kyung Hee University, 1732 Deogyeong-daero, Giheung-gu, Yongin-si, Gyeonggi-do 17104, Republic of Korea

ARTICLE INFO

Keywords:
Microfluidic pneumatic circuit
Plasma separation
Vacuum pillar
Thrombin
Aptamer beacon

ABSTRACT

Developing simple, portable, rapid, and easy-to-use diagnostic technologies is essential for point-of-care (POC) blood molecular testing. Integrated microfluidic devices that include the functionalities of blood separation, microfluidic pumping, and molecular detection are desirable for POC testing; however, current technologies still rely on off-chip sample processing or require bulky equipment. We report a fully-integrated microfluidic diagnostic device, i.e., an integrated pneumatic microfluidic circuit (iPC), that can autonomously pump whole blood, continuously sort blood plasma, and readily enable blood plasma proteomic analysis. The iPC contains vacuum pillars as a vacuum source and waste reservoir, as well as microchannels connecting the pillars as a plasma separator or a flow stabilizer. We combined the iPC and a miniaturized fluorescence microscope to create a portable diagnostic platform that enables fluorescence-based biomarker detection. First, we performed systematic parametric studies to establish design rules for determining the transport and distribution of fluid streams in the iPC. We then demonstrated the capability of the iPC-based diagnostic platform by successfully separating blood plasma from microliter quantities of whole blood while simultaneously quantifying thrombin in blood samples using an aptamer beacon within 5 min of sample injection. Our platform holds potential as a rapid, field-deployable, essentially universal diagnostic tool in POC settings.

1. Introduction

Molecular diagnostics using blood can provide the molecular signatures of various maladies such as infection, inflammation, and tumor progression reflecting physiological and pathological conditions. This facilitates disease diagnosis, prognosis, and monitoring of responses to therapy (Cohen et al., 2018; Meany et al., 2009; Song et al., 2014; Weiner et al., 2018). Rapid, point-of-care (POC) assays are ideal for blood tests that target plasma molecules, which can be unstable; for example, plasma proteins can rapidly degrade after blood collection (Hsieh et al., 2006) and the half-life of cell-free DNA is known to range from minutes to hours (Khier and Lohan, 2018; Volik et al., 2016). Lateral flow test strips (LFTSs) and more advanced microfluidic paper-based analytical devices (μPADs) have unique features suitable for POC testing (POCT), such as cost-effectiveness, ease of use, and portability (Noiphung et al., 2013; Tseng et al., 2018; Yang et al., 2012). However, most LFTSs are qualitative or semi-quantitative, and both LFTSs and μPADs often lack the ability to sort blood cells from whole blood which can interfere with optical and electrical readouts. Integration of a filter paper or an agglutinating antibody into μPADs enables effective blood cell separation (Noiphung et al., 2013; Tseng et al., 2018; Yang et al., 2012) but can pose a risk of hemolysis, (Son et al., 2014) which can produce assay inhibitors.

Integrated microfluidic devices capable of on-chip blood plasma separation and in-situ molecular detection have demonstrated several advantages for POCT, such as integrating sample preparation and analysis protocols, eliminating the necessity of off-chip transfer of blood samples, and enabling rapid analysis (Betancur et al., 2017; Dimov et al., 2011; Fan et al., 2008; Koh et al., 2015; Lee et al., 2009, 2018; Schaff and Sommer, 2011; Wang et al., 2010; Yeh et al., 2017). The typical structure of integrated devices contains three major components: (i) a pumping mechanism, such as a syringe pump (Fan et al., 2008), gas-permeable silicone-based vacuum pump (Dimov et al., 2011; Yeh et al., 2017), capillary pump (Betancur et al., 2017; Wang et al., 2010), water-head pump (Lee et al., 2018), or centrifugal pump (Koh et al., 2015; Lee et al., 2009; Schaff and Sommer, 2011); (ii) a separation mechanism, such as Zweifach-Fung effect-based microfluidic separation (Fan et al., 2008), inertial separation (Wang et al., 2010), gravitational sedimentation (Dimov et al., 2011; Yeh et al., 2017), dead-end filtration (Lee et al., 2018) or centrifugal separation (Koh et al., 2015; Lee et al., 2009; Schaff and Sommer, 2011); and (iii) a molecular analysis modality, such as immuno-fluorescence (Fan et al.,

* Corresponding authors.
E-mail addresses: yj8407@khu.ac.kr (Y.-J. Kim), s.choi@khu.ac.kr (S. Choi).

https://doi.org/10.1016/j.bios.2019.03.018
Received 24 January 2019; Received in revised form 9 March 2019; Accepted 11 March 2019
Available online 12 March 2019

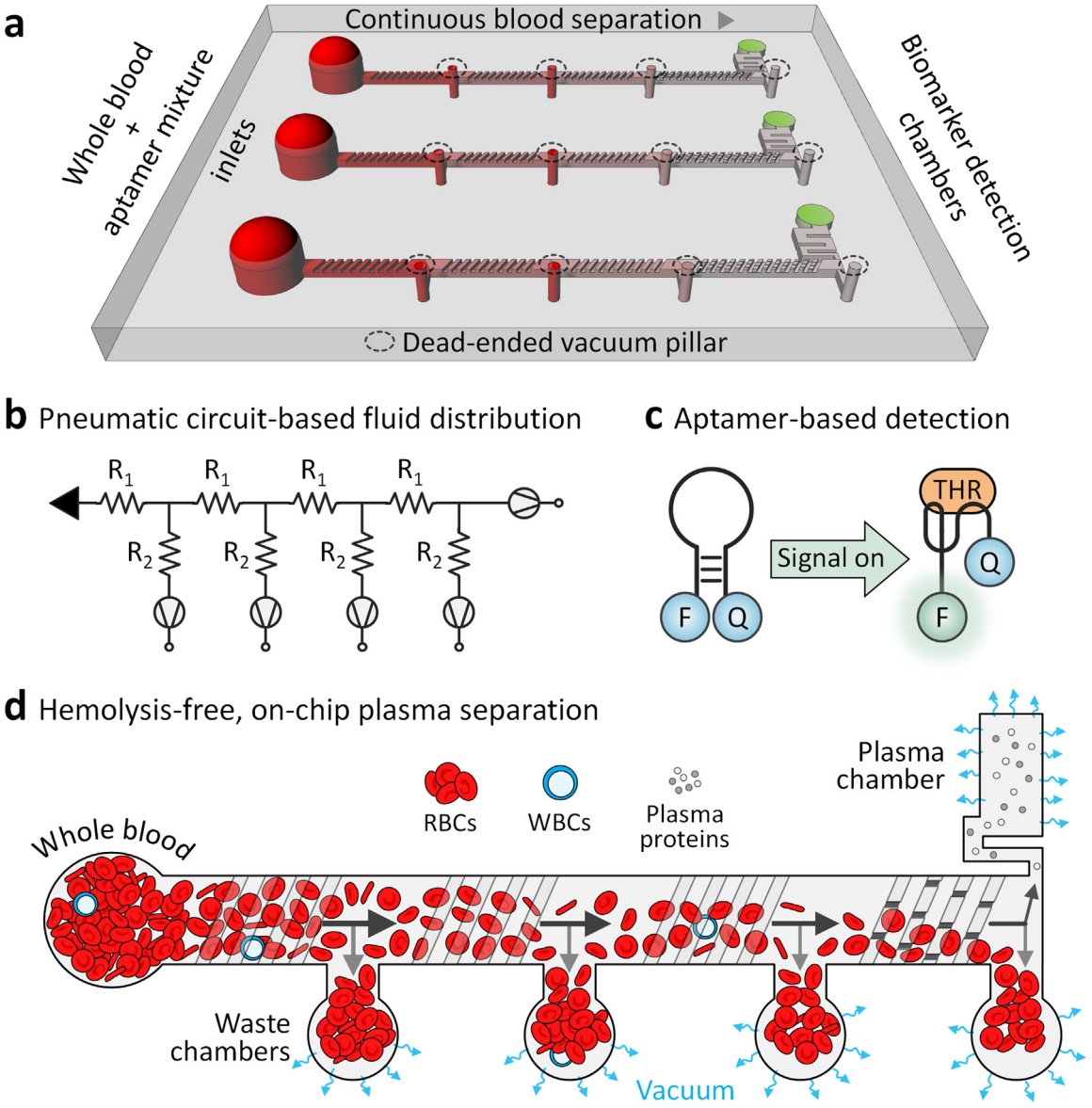

Fig. 1. Integrated pneumatic microfluidic circuit (iPC) including the functionalities of microfluidic pumping, blood separation, and molecular detection. (a) In the straightforward user protocol, a mixture of blood and reagent is dropped onto the inlet, followed by automatic sample preparation and biomarker detection. (b) A pneumatic circuit diagram of the iPC consisting of vacuum source (i.e., vacuum pillars or a plasma chamber) and fluidic resistors (i.e., separation or interconnection channels) provides a basic understanding of how fluid streams are autonomously distributed into the channel ends. (c) Binding of the aptamer beacon to the target molecule, (i.e., thrombin (THR)) results in conformational change, which increases the distance between a fluorescence dye (F) and a quencher (Q) at the ends of the aptamer beacon, and thereby generating fluorescence that can be detected. (d) Slant ridge-patterned microchannels autonomously remove blood cells by hydrophoresis to the vacuum pillars and direct blood plasma into the plasma chamber. Channel and groove dimensions are not scaled.

2008; Koh et al., 2015; Schaff and Sommer, 2011; Wang et al., 2010), field-effect transistor-based biosensing (Betancur et al., 2017), enzyme-linked immuno-sorbent assay (Lee et al., 2009) or isothermal amplification (Lee et al., 2018; Yeh et al., 2017). These devices can be classified into active and passive depending on pumping mechanism. Active systems based on external driving forces have the advantage of easily adopting existing separation methods and achieving effective blood separation; however, they require bulky instrumental set-ups that can limit their use for POCT applications. Passive systems based on gas-permeable materials or capillary wicking structures typically use a single linear channel with a blocked outlet. Due to their limited pumping ability to direct multiple separation streams into designated outlets, these rely on simpler separation principles, such as dead-end filtration or gravitational sedimentation. However, using a filter can cause hemolysis by clogging if the hematocrit level is high (Son et al., 2014). This filtration also requires an additional process for inserting the filter. In addition, most integrated devices have demonstrated their diagnostic capability using bench-top equipment, such as a microscope or a microarray scanner. Therefore, it is necessary to verify their applicability to POCT using a portable reader.

To mitigate the above challenges, we present a fully-integrated microfluidic diagnostic device, i.e., an integrated pneumatic microfluidic circuit (iPC) that enables autonomous pumping, directed fluid distribution into multiple outlets, hemolysis-free and on-chip blood plasma separation, and portable signal readout combined with a miniaturized fluorescence microscope (Fig. 1). To the best of our knowledge, this is the first report to provide design rules for determining the transport and distribution of fluid streams in an iPC with a microfluidic network composed of multiple vacuum pillars as a vacuum source and waste outlet. Based on the design rules, we can adopt a continuous-flow

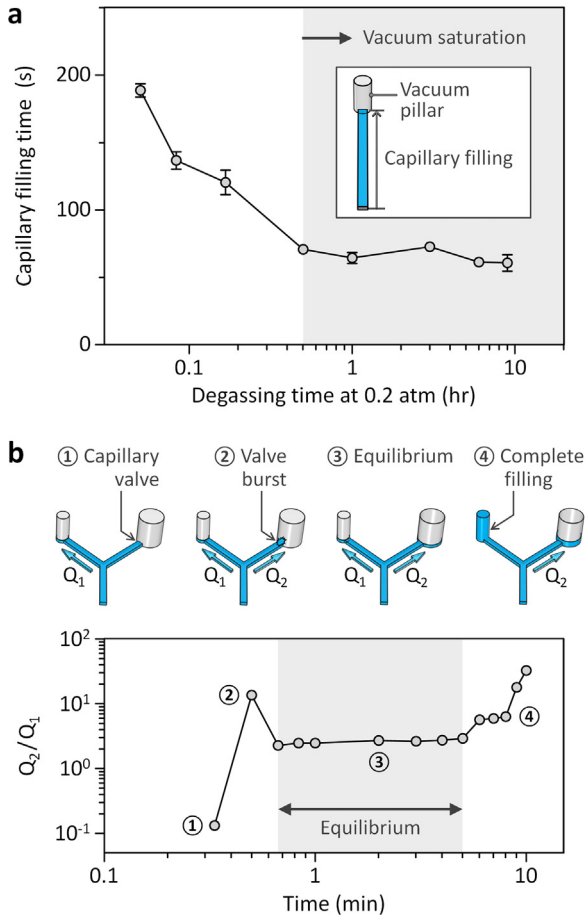

Fig. 2. Characterization of vacuum-driven microflows with DI water. (a) Effect of PDMS degassing time on vacuum level in the vacuum pillar and speed of capillary filling under vacuum. The capillary was 200 μm in width, 30 μm in height, and 2 cm in length. The diameter of the vacuum pillar was 0.5 mm. (b) Distribution kinetics of vacuum-driven fluid streams at the branch of the Y-shaped microchannel can be affected by the capillary valve effect, valve burst, and complete filling of a vacuum pillar. The diameters of the vacuum pillars on the left and right sides were 0.5 mm and 1.5 mm, respectively.

microfluidic separation principle easily into the iPC, which has not been achieved before. After optimizing the iPC design, we successfully isolated blood plasma from whole blood with high purity (over 99.9%) and demonstrated in-situ, quantitative analysis of thrombin in blood samples using an aptamer beacon. The iPC represents a universal platform to convert existing microfluidic devices requiring pumping equipment into autonomous devices suitable for POC applications.

2. Material and methods

2.1. Device design and fabrication

Three different types of polydimethylsiloxane (PDMS) devices were fabricated to characterize vacuum-driven microflows in simple pneumatic microfluidic circuits and the iPC. The simple characterization devices are 1-cm-long or 2-cm-long linear channels with a vacuum pillar at the end of the channel and a Y-shaped microchannel (8 mm from the inlet to the branch and 2 mm from the branch to each vacuum pillar). The iPC consists of vacuum pillars, separation channels and a plasma chamber. For device fabrication, photoresist (SU-8 2015; Microchem Corp., United States) microstructures were fabricated on a silicon wafer using standard photolithography. The photolithography process was repeated to create a multi-layer microchannel for the iPC. Each photoresist (PR) layer was fabricated by PR spin coating, soft baking (65 °C for 10 min and 95 °C for 40 min) to reduce residual solvent, ultraviolet exposure (7 s) through a photomask, baking (95 °C for 30 min) to remove residual solvent and solidify the exposed PR patterns, and removal of unexposed PR with a developer solution. The spin-coating condition for the characterization devices was 2700 rpm for 35 s. In the iPC mold, the first PR layer comprised flat channel structures 12 μm in height, and the second layer was slant ridge patterns 18 μm in height. The corresponding spin-coating conditions for the first and second layers were 3300 rpm for 35 s and 3100 rpm for 35 s, respectively. After silanization of the PR molds, channel patterns were transferred to PDMS by pouring a mixture of PDMS and its curing agent (at a 10:1 (wt/wt) ratio) into the molds at a thickness of 1.2 mm. PDMS was cured at 75 °C for 1 h, cut into individual devices, and punched to form inlet and outlet holes for fluidic access and vacuum pillars, respectively. An inlet hole (3 mm in diameter) and vacuum pillars (a dimeter range of 0.5–2 mm) were manually generated by punching the PDMS devices using biopsy punches with diameters corresponding to the punched diameters. Misalignment between a vacuum pillar and the corresponding microchannel structure did not significantly affect vacuum-driven pumping, flow distribution and plasma separation in the iPC. Their precise alignment can be achieved by creating the photoresist structures of the vacuum pillars with additional photolithography. Then, each device was placed on a glass slide without any surface treatment. Its top surface, except at the inlet, was covered with a cover glass. Before all experiments, the PDMS devices were degassed in a vacuum chamber for a set period of time (Fig. S1).

2.2. Sample preparation and analysis

Canine blood samples were purchased from the Korea Animal Blood Bank in compliance with safety regulations, and the level of hematocrit was between 42% and 45% when measured as the ratio of length of packed red blood cells to length of injected blood sample in a capillary tube after centrifugation. To evaluate the plasma separation performance of the iPC, plasma purity was determined as the ratio of number of removed blood cells in the plasma chamber to initial total number of blood cells. For the hemolysis test, a hemolyzed blood sample was prepared by treating whole blood with an RBC lysis buffer (Biolegend, Inc., USA). Then, spectral analysis of blood samples was performed in the plasma chamber of the iPC with a spectrometer (Ocean Optics, Inc., United States) equipped with a bench-top microscope (Nikon Corp., Japan). For thrombin assays, an aptamer beacon with a specific binding affinity for thrombin was synthesized by coupling fluorescein at the 5′-end and a BHQ-1 (black hole quencher-1) group at the 3′-end (Bioneer, Inc., Korea). The aptamer beacon was heated to 99 °C for 3 min and cooled to 25 °C prior to experiments. The sequence of the aptamer beacon is CCAACGGTTGGTGTGGTTGG, which forms a quenched stem-loop conformation without the target (Hamaguchi et al., 2001). Target-induced conformation changes distance the fluorescent dye and the quencher, thereby generating florescence signals. Whole blood was washed with DPBS (Dulbecco's Phosphate Buffered Saline) and re-suspended in Tris buffer (10 mM Tris-HCl at pH 7.5, supplemented with 0.1 mM EDTA and 0.1% bovine serum albumin) to prevent coagulation when thrombin and blood were mixed. Then, thrombin molecules were spiked into the washed blood samples at varying concentrations. Before conducting thrombin assays with the iPC, the aptamer beacon was spiked in the model blood sample at a concentration of 3 μM. The limit of detection (LOD) for the thrombin assay is determined as $3\sigma_b/s$, where σ_b is the standard deviation for blank measurements and s is the slope of the linear detection range.

2.3. Experimental setup

All experiments were performed by dropping a liquid sample onto the inlet of a device without external pumps. The distribution ratio of volumetric flow rates of fluid streams at the branch point of the Y-

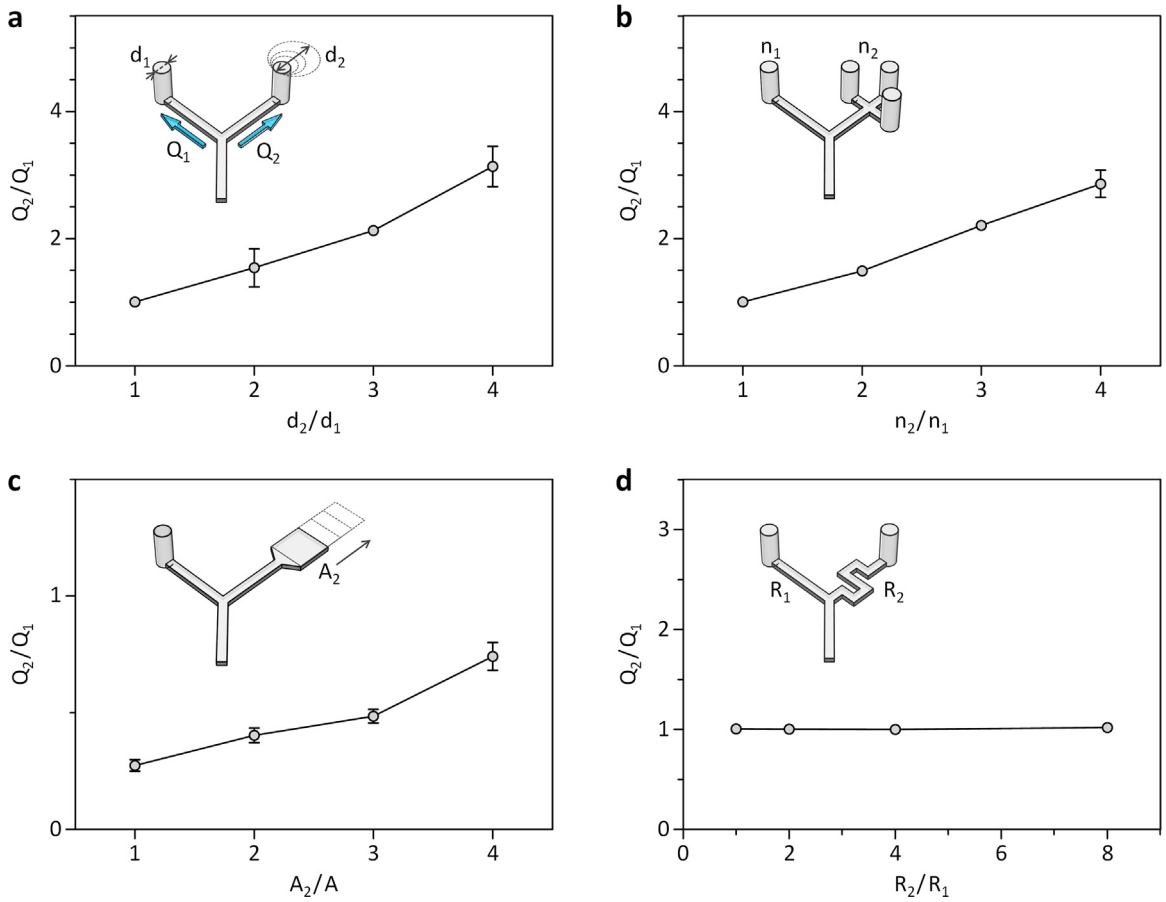

Fig. 3. Experimental investigation of multiple design parameters determining fluid transport and distribution in the iPC with DI water. (a, b, c) The volumetric flow rate to the vacuum pillar or the microchamber of the Y-shaped microchannel is linearly proportional to (a) pillar diameter (*d*), (b) number of pillars (*n*), and (c) surface area (*A*) of the microchamber. These parameters are a major consideration for designing an iPC. (d) The difference in hydraulic resistance (*R*) from the branch of the Y-shaped microchannel to each vacuum pillar has no effect on the distribution of vacuum-driven fluid streams. The left vacuum pillar of the microchannel was fixed with $d_1 = 0.5$ mm for all experiments.

shaped channel was determined by spiking 1 μm fluorescent microparticles into deionized (DI) water and observing the strikelines of the particles using a bench-top fluorescence microscope (Nikon). As a portable fluorescence reader, a miniaturized fluorescence microscope was fabricated by assembling an LED (470 nm; LED Engin, Inc., United States), optical filters with 460 nm and 609 nm center wavelengths (Semrock, Inc., United States), a 10 × objective lens (Newport Corp., United States), a dichroic mirror (Semrock, Inc., United States), and a CMOS sensor (PCO AG, Germany). These optical components were compactly assembled using lens tubes (Thorlabs, Inc., United States) and a 3D-printed housing. Captured fluorescence images were analyzed using ImageJ software (National Institutes of Health, United States).

3. Results and discussion

3.1. Design rules for integrated pneumatic circuits

A partial vacuum generated by absorption of air molecules into degassed PDMS is an ideal source for passive microfluidic pumping and has been exploited for POC applications (Xu et al., 2015). Although many efforts have been made to understand the underlying mechanisms of air diffusion through PDMS and the resulting vacuum-driven pumping (Han et al., 2007; Hosokawa et al., 2004; Li et al., 2012; Xu et al., 2015), these studies are mainly limited to simple linear channels. Comprehensive understanding of fluid transport and distribution in a vacuum-driven pneumatic channel circuit with multiple bifurcations and vacuum pillars remains elusive. This limitation is a major cause of difficulties in applying previous microfluidic technologies (i.e., continuous-flow blood plasma separation technologies) into pneumatic channel circuits. Thus, we first performed a parametric study to identify key factors to determine the ratio at which a fluid divides into multiple streams at the branches of the pneumatic channel circuit. For this, we examined how fast PDMS can be fully outgassed by measuring the time (τ_c) required to fill the dead-ended capillary with a vacuum pillar. As shown in Fig. 2a, τ_c decreases with PDMS degassing time and becomes constant after 30 min of degassing. To maintain a constant vacuum, we used PDMS devices after degassing them for more than 1 h. We then studied the effects of various design parameters, such as diameter of a vacuum pillar (*d*), number of vacuum pillars (*n*), surface area (*A*) of a microchamber, and hydraulic resistance from the branch of the Y-shaped microchannel to a vacuum pillar (*R*) on fluid distribution. Since the distribution ratio of volumetric flow rates (Q_2/Q_1) at the branch point can be affected by the capillary-valve effect, which is a phenomenon where the flow of liquid can stop as the channel cross-section is suddenly changed, we measured Q_2/Q_1 at the equilibrium state when both vacuum pillars were partially filled with liquid; the ratio became constant (Fig. 2b). As shown in Fig. 3, Q_2/Q_1 increased linearly in proportion to *d*, *n*, and *A*; however, it was independent of *R*. These results can be explained as a larger *A* increasing the amount of air absorbed, allowing a stronger vacuum to be formed (Hosokawa et al., 2004).

$$Q \propto FA = \frac{2AD\Delta C}{l}\exp(-t/\tau) \quad (1)$$

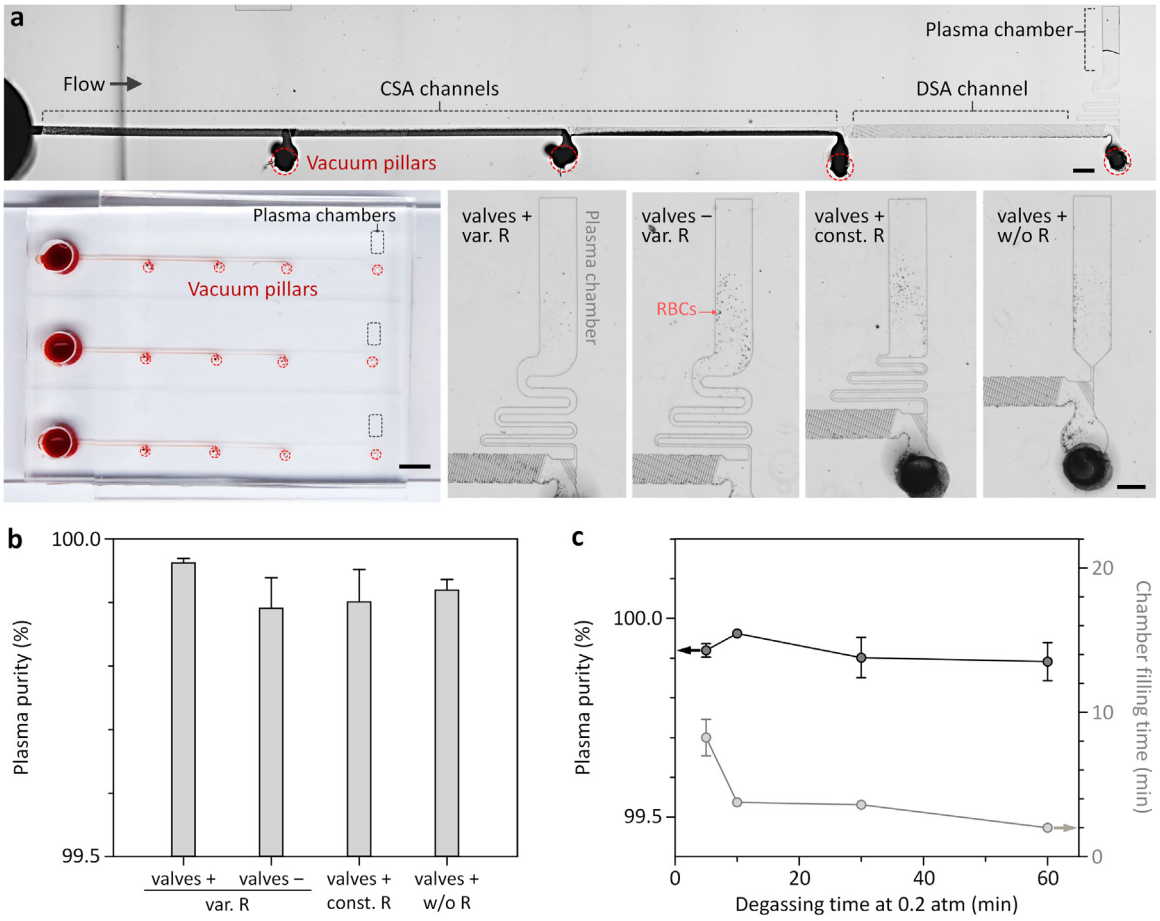

Fig. 4. Blood plasma separation using the iPC. (a) (Top) Micrograph of the blood separation process in the iPC consisting of three CSA channels and one DSA channel. Scale bar, 500 μm. (Bottom left) Three separate whole-blood samples can be processed at once. Scale bar, 3 mm. (Bottom right) Four different separator designs with different combinations of capillary valves and interconnection channels between the last valve and the plasma chamber. Scale bar, 300 μm. (b) Effect of separator design on plasma purity. (c) Effect of PDMS degassing time on the plasma purity and plasma separation time (i.e., the time it takes the sorted blood plasma to fill the plasma chamber).

where F is the air flux at the PDMS surface, D is the diffusion coefficient of air in PDMS, ΔC is the difference in air concentration between atmospheric and vacuum environments, l is the thickness of the PDMS substrate, and τ is the characteristic time constant. As normalized in terms of A, the data sets for d, n, and A show a linear correlation, with an R^2 value of 0.9692 (Fig. S2). This demonstrates that A is an important design parameter for determining Q_2/Q_1. We note that Q_2/Q_1 is unprecedentedly unaffected by R, which is a typical determinant of the volumetric rate of a pressure-driven flow. The reason for this is likely that the vacuum pressure (ΔP_v) in a vacuum pillar can be rapidly saturated and depends on R. ΔP_v can be defined as (Truskey et al., 2009)

$$\Delta P_V = \Delta P_d - P_C = \frac{S\mu}{D_h^2} L(t) v(t) - 2\gamma \cos\theta \left(\frac{1}{h} + \frac{1}{w}\right) \quad (2)$$

where ΔP_d is the pressure drop between the inlet and advancing front of the liquid; P_c is the capillary pressure; $L(t)$ is the fluid length inside the channel at a given time; $v(t)$ is the fluid velocity at a given time; S is a constant related to the channel geometry; μ is the fluid viscosity; and D_h is the hydraulic diameter of the channel, which is defined as $D_h = 2hw/(h + w)$; h and w are the channel height and width, respectively; γ is the surface tension of the fluid; and θ is the contact angle of the fluid flowing though the PDMS microchannel. In dead-ended capillaries (1 cm and 2 cm in length) with a vacuum pillar, saturated ΔP_v is proportional to hydraulic resistance (Fig. S3). The higher is R, the higher is the saturated ΔP_v; thus, even though one channel has a higher R, fluid can flow at the same flow rate through both branched channels (Fig. 2d). These findings indicate the following design rules for a vacuum-driven pneumatic channel circuit.

1. The A of vacuum pillars and microchambers is a major consideration when designing the pneumatic channel circuit. The volumetric flow rate to vacuum pillars or microchambers is linearly proportional to their surface area.
2. R has no effect on fluid distribution in the pneumatic channel circuit. This means that we can freely insert a desired channel (e.g., microfluidic separators) between a channel branch in the channel circuit and a vacuum pillar without affecting the circuit design.

3.2. Integration of a pneumatic microfluidic circuit and a microfluidic separator

We applied the established design rules to the iPC for continuous-flow plasma separation and in-situ molecular detection. The iPC is a dead-end microfluidic network in which vacuum pillars are arranged at regular intervals, and separation channels patterned with slant ridges are connected between the pillars (Fig. 4a). We adopted an autonomous cell separation technology, referred to as hydrophoresis, in the iPC to harness the advantages of continuous-flow, passive cell separation, such as hemolysis-free separation and easy device fabrication without additional filter assembly (Kim et al., 2016, 2017, 2018; Yan et al., 2014). For continuous-flow blood plasma separation by hydrophoresis, the first three separation channels from the inlet are designed with

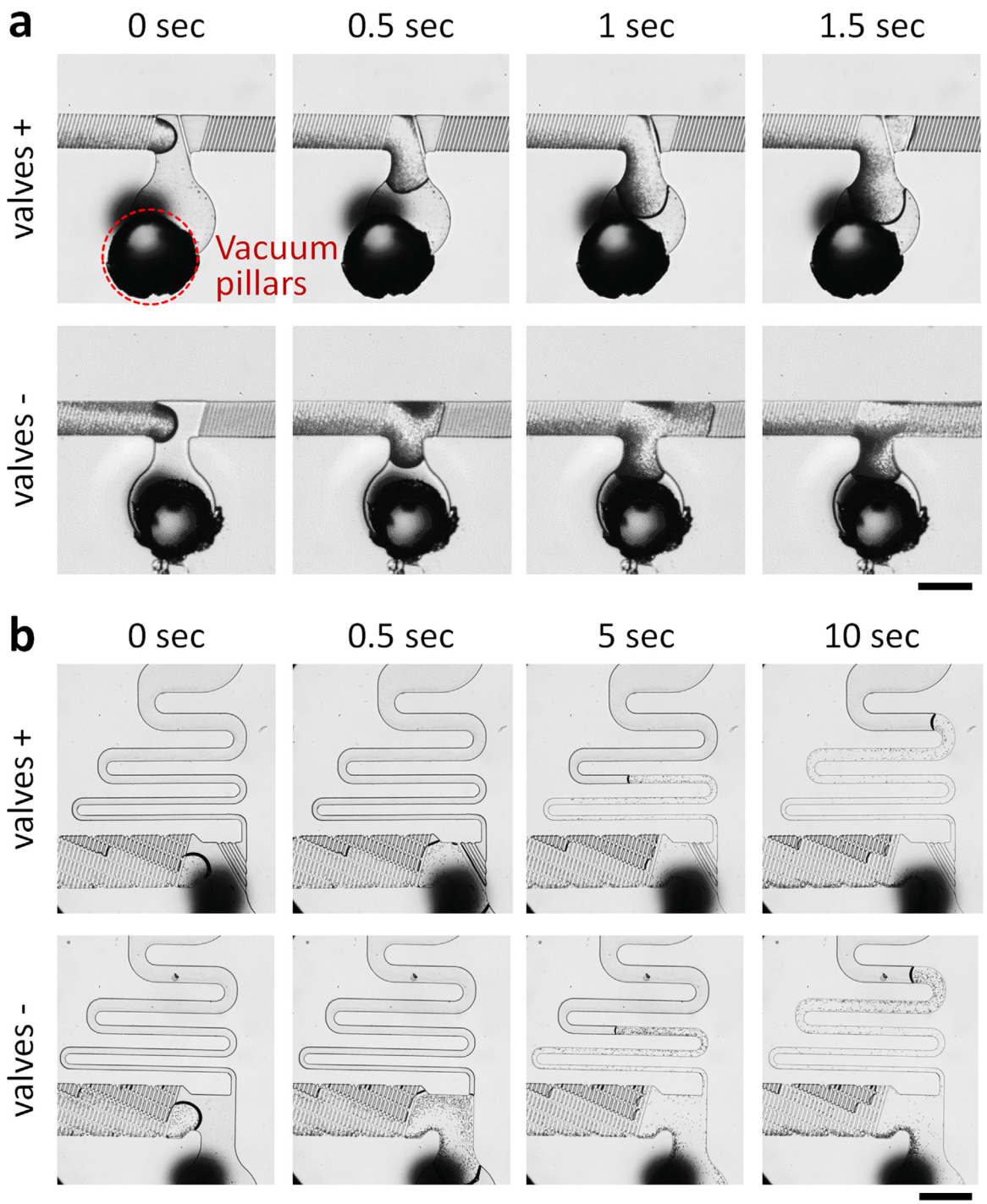

Fig. 5. Effect of capillary valve on plasma separation. (a) The slant capillary valve directs the leading front of the blood flow to the vacuum pillar, preventing inflow of blood streams containing blood cells into the next separation channel. (b) The capillary-valve effect lowers the amount of blood cells in the advancing front of the blood flow as it moves downstream, finally obtaining high-purity blood plasma in the plasma chamber. Scale bars, 300 μm.

continuous slant ridges (CSAs), and the last channel is patterned with discontinuous slant ridges (DSAs) (Fig. 4a and S4). The slant ridges on the channel top can generate secondary flows, superimposing a rotational flow pattern onto the axial flow (Stroock et al., 2002). Additionally, the channel dimension (i.e., height) similar to the cell size allows the cells to be sterically controlled outside the ridges and located under the ridge structure. These two combined effects make it possible to focus blood cells at an angle opposite the inclination angle of the ridges (Fig. 1d), directing them into the vacuum pillars. We also designed four vacuum pillars (d = 0.5 mm) in the iPC, where the A of the plasma chamber is two times smaller than the A of the vacuum pillar. Thus, less than 10% of the injected blood flow can be directed into the plasma chamber, which corresponds to the plasma recovery efficiency of previous hydrophoresis plasma separators (Kim et al., 2017). We note that additional secondary flows driven by the non-uniform surface tension at the advancing front of the blood flow can affect plasma purity (φ) by directing some blood cells into the plasma chamber (Figs. 4a, b, and 5). Placing a capillary valve before the next separation channel or plasma chamber can direct the leading front of the blood flow toward the vacuum pillars, thereby improving φ. In addition,

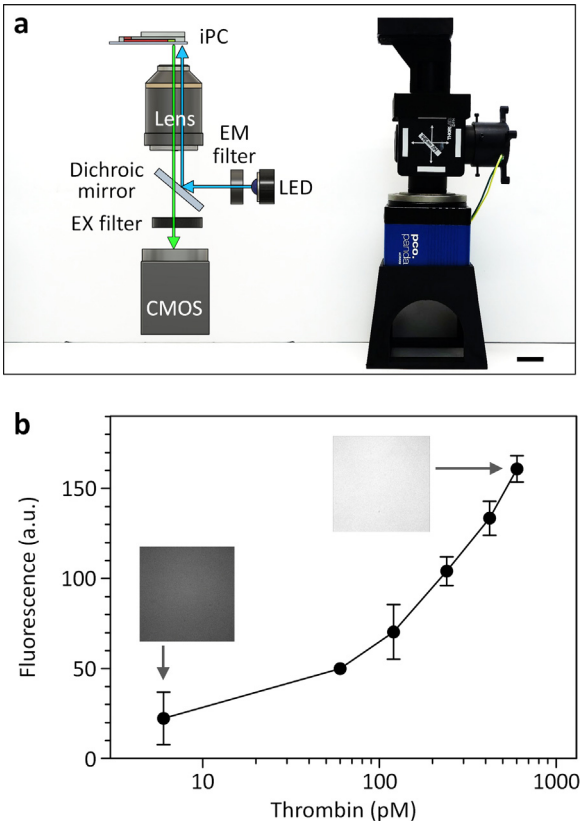

Fig. 6. Point-of-care testing of thrombin using the iPC. (a) Miniaturized fluorescence microscope consisting of a light-emitting diode, optical filters, a dichroic mirror, an objective lens, a CMOS sensor, and a 3D-printed sample mount for portable signal readout of aptamer-based bioassays. Scale bar, 2 cm. (b) Correlation of the fluorescence signal and corresponding thrombin concentration. Blood samples spiked with varying concentrations of thrombin were automatically processed in the iPC. Then, the binding events between the aptamer beacon and the target biomarker were measured in situ using the miniaturized fluorescence microscope. The insets show representative fluorescence micrographs taken using the microscope at corresponding thrombin concentrations.

connecting the plasma chamber with a microchannel that has a gradually increasing width can reduce the sudden inflow of blood containing cells into the plasma chamber by the capillary-valve burst; again, this improves φ (Fig. 4b). Using the optimized design with the capillary valves and the connecting channel that increases in width, we achieved high-purity plasma separation from a drop of whole blood (3 μL) with φ greater than 99.8%, regardless of ΔP_v (Fig. 4c). To assess hemolysis, we performed spectral analysis of hemoglobin species in the plasma chamber of the iPCs loaded with whole blood, hemolyzed blood, and centrifuged plasma. As a direct evidence of hemolysis, the hemoglobin absorbance (541 and 576 nm) can be used to determine whether hemolysis occurred during plasma separation. As shown in Fig. S5, the characteristic absorbance peaks were observed only in hemolyzed blood but not in on-chip sorted and centrifuged plasma, indicating that the iPC offers a simple and gentle plasma separation method without hemolysis as well as providing a passive pumping method.

3.3. In-situ thrombin detection from blood using the integrated pneumatic circuit

Finally, we integrated an aptamer-based biosensing platform with the iPC. The biosensing platform uses an aptamer beacon with a specific binding affinity for thrombin as a bio-transducer and a miniaturized fluorescence microscope as a portable signal reader (Fig. 6). Aptamer beacons are suitable for realizing point-of-care molecular diagnostics in the iPC because they can directly transduce target binding into an easily measurable signal (e.g., fluorescence) without requiring additional sample preparation steps such as target labeling or washing (Deng et al., 2014; Hamaguchi et al., 2001). To prevent coagulation when thrombin and blood are mixed, we washed whole blood samples two times and then spiked thrombin molecules into the washed blood samples. As a model system for diagnosis of coagulation abnormalities (Chung et al., 2018; Muller et al., 2011), we successfully detected thrombin level in the final blood samples via on-chip blood separation and in-situ fluorescence detection in the iPC (Fig. 6b), showing a dynamic range up to 600 pM, which corresponds to a high level of thrombin in patient blood samples (Muller et al., 2011). Thrombin assays were performed by simply dropping 3 μL of a blood sample onto the inlet of the iPC and measuring the fluorescence intensity within 5 min of sample loading. The limit of detection (LOD) was calculated to be 133.37 pM, which is higher than the typical plasma level (less than 1 pM) in healthy individuals (Muller et al., 2011). Thus, further improvement in LOD is required to differentiate patients and healthy individuals. The proposed platform exhibits moderate detection performance (LOD = 133.37 pM) as compared with existing aptamer-based sensors: 490 pM for an aptamer-based amperometric sensor (Chung et al., 2018) and 0.47 pM for an aptamer-based enzyme assay (Muller et al., 2011). Adopting enzyme-based signal-amplification strategies can improve the LOD of the iPC by continuously generating fluorescent products (Muller et al., 2011). In addition, further improvement in LOD can be achieved by incorporating microfluidic molecular pre-concentrators into the iPC platform and thus increasing the local concentration of thrombin (Cheow et al., 2010; Oh et al., 2016). If the concentration of thrombin exceeds 600 pM, the fluorescence signal will saturate under the current fluorescence imaging settings (i.e., exposure time and gain), thus limiting the detection range. Given that aptamer sensors for thrombin detection can detect nanomolar ranges (Chung et al., 2018), extending the dynamic range of the iPC can be achieved by adjusting the imaging settings. Based on the various aptamer sensors developed so far, our iPC platform can be easily extended to POC detection of many diseases beyond thrombin diagnosis. The iPC can be vacuum-packed to eliminate the need for additional bulky vacuum equipment when end-users use the devices. Instead of vacuum pillars, capillary pumps based on wicking structures can be used for constructing the iPC, thus fundamentally eliminating the need for vacuum equipment and the degassing process.

4. Conclusion

In summary, we established design rules by which fluid transport and distribution in a vacuum-driven pneumatic channel circuit can be determined. We applied these design rules to develop an integrated pneumatic microfluidic circuit capable of autonomous micropumping, on-chip, hemolysis-free blood separation, and in-situ molecular detection, which can enable rapid POC testing from a tiny amount of blood obtained by a finger prick. We believe our investigation into vacuum-driven microfluidics will have broad implications for extending its applications with more complex channel networks and functionalities. As an example of such applications, the integrated microfluidic circuit represents a portable diagnostic platform for rapid and reliable detection of fragile biomarkers that can be easily degraded in sampled blood. Based on the simplicity, portability, and quantitative molecular detection demonstrated, POC testing with the iPC could be performed at the patient's bedside to continuously provide diagnostic information for therapeutic intervention.

CRediT authorship contribution statement

Suyeon Shin: Conceptualization, Investigation, Methodology, Visualization, Writing - original draft, Writing - review & editing. **Byeongyeon Kim:** Data curation, Methodology, Formal analysis. **Yoon-Jin Kim:** Funding acquisition, Methodology, Supervision. **Sungyoung Choi:** Conceptualization, Funding acquisition, Project administration, Resources, Supervision, Writing - original draft, Writing - review & editing.

Acknowledgements

This research was supported by Basic Science Research Program through the National Research Foundation of Korea (NRF) funded by the Ministry of Science, ICT & Future Planning (MSIP) (2015R1C1A1A01053990), and a NRF grant funded by the MSIP (2016R1A5A1010148). YJK was supported by a NRF grant funded by the MSIP (2018R1C1B6005346).

Declaration of interests

None.

Appendix A. Supplementary material

Supplementary data associated with this article can be found in the online version at doi:10.1016/j.bios.2019.03.018.

References

Betancur, V., Sun, J., Wu, N., Liu, Y., 2017. Integrated lateral flow device for flow control with blood separation and biosensing. Micromachines 8 (12), 367.
Cheow, L.F., Ko, S.H., Kim, S.J., Kang, K.H., Han, J., 2010. Increasing the sensitivity of enzyme-linked immunosorbent assay using multiplexed electrokinetic concentrator. Anal. Chem. 82 (8), 3383–3388.
Chung, S., Moon, J.M., Choi, J., Hwang, H., Shim, Y.B., 2018. Magnetic force assisted electrochemical sensor for the detection of thrombin with aptamer-antibody sandwich formation. Biosens. Bioelectron. 117, 480–486.
Cohen, J.D., Li, L., Wang, Y.X., Thoburn, C., Afsari, B., Danilova, L., Douville, C., Javed, A.A., Wong, F., Mattox, A., Hruban, R.H., Wolfgang, C.L., Goggins, M.G., Dal Molin, M., Wang, T.L., Roden, R., Klein, A.P., Ptak, J., Dobbyn, L., Schaefer, J., Silliman, N., Popoli, M., Vogelstein, J.T., Browne, J.D., Schoen, R.E., Brand, R.E., Tie, J., Gibbs, P., Wong, H.L., Mansfield, A.S., Jen, J., Hanash, S.M., Falconi, M., Allen, P.J., Zhou, S., Bettegowda, C., Diaz, L.A., Tomasetti, C., Kinzler, K.W., Vogelstein, B., Lennon, A.M., Papadopoulos, N., 2018. Detection and localization of surgically resectable cancers with a multi-analyte blood test. Science 359 (6378), 926–930.
Deng, B., Lin, Y., Wang, C., Li, F., Wang, Z., Zhang, H., Li, X.F., Le, X.C., 2014. Aptamer binding assays for proteins: the thrombin example–a review. Anal. Chim. Acta 837, 1–15.
Dimov, I.K., Basabe-Desmonts, L., Garcia-Cordero, J.L., Ross, B.M., Park, Y., Ricco, A.J., Lee, L.P., 2011. Stand-alone self-powered integrated microfluidic blood analysis system (SIMBAS). Lab Chip 11 (5), 845–850.
Fan, R., Vermesh, O., Srivastava, A., Yen, B.K., Qin, L., Ahmad, H., Kwong, G.A., Liu, C.C., Gould, J., Hood, L., Heath, J.R., 2008. Integrated barcode chips for rapid, multiplexed analysis of proteins in microliter quantities of blood. Nat. Biotechnol. 26 (12), 1373–1378.
Hamaguchi, N., Ellington, A., Stanton, M., 2001. Aptamer beacons for the direct detection of proteins. Anal. Biochem. 294 (2), 126–131.
Han, Z., Tang, X., Zheng, B., 2007. A PDMS viscometer for microliter newtonian fluid. J. Micromech. Microeng. 17 (9), 1828–1834.
Hosokawa, K., Sato, K., Ichikawa, N., Maeda, M., 2004. Power-free poly(dimethylsiloxane) microfluidic devices for gold nanoparticle-based DNA analysis. Lab Chip 4 (3), 181–185.
Hsieh, S.Y., Chen, R.K., Pan, Y.H., Lee, H.L., 2006. Systematical evaluation of the effects of sample collection procedures on low-molecular-weight serum/plasma proteome profiling. Proteomics 6 (10), 3189–3198.
Khier, S., Lohan, L., 2018. Kinetics of circulating cell-free DNA for biomedical applications: critical appraisal of the literature. Future Sci. OA 4 (4), Fso295.
Kim, B., Choi, Y.J., Seo, H., Shin, E.C., Choi, S., 2016. Deterministic migration-based separation of white blood cells. Small 12 (37), 5159–5168.
Kim, B., Oh, S., You, D., Choi, S., 2017. Microfluidic pipette tip for high-purity and high-throughput blood plasma separation from whole blood. Anal. Chem. 89 (3), 1439–1444.
Kim, B., You, D., Kim, Y.-J., Oh, I., Choi, S., 2018. Motorized smart pipette for handheld operation of a microfluidic blood plasma separator. Sens. Actuators B: Chem. 267, 581–588.
Koh, C.Y., Schaff, U.Y., Piccini, M.E., Stanker, L.H., Cheng, L.W., Ravichandran, E., Singh, B.R., Sommer, G.J., Singh, A.K., 2015. Centrifugal microfluidic platform for ultra-sensitive detection of botulinum toxin. Anal. Chem. 87 (2), 922–928.
Lee, B.S., Lee, J.-N., Park, J.-M., Lee, J.-G., Kim, S., Cho, Y.-K., Ko, C., 2009. A fully automated immunoassay from whole blood on a disc. Lab Chip 9 (11), 1548–1555.
Lee, Y., Kim, D.M., Li, Z., Kim, D.E., Kim, S.J., 2018. Pulsatile plasma filtration and cell-free DNA amplification using a water-head-driven point-of-care testing chip. Lab Chip 18 (6), 915–922.
Li, G., Luo, Y., Chen, Q., Liao, L., Zhao, J., 2012. A "place n play" modular pump for portable microfluidic applications. Biomicrofluidics 6 (1), 14118–1411816.
Meany, D.L., Sokoll, L.J., Chan, D.W., 2009. Early detection of cancer: immunoassays for plasma tumor markers. Expert Opin. Med. Diagn. 3 (6), 597–605.
Muller, J., Becher, T., Braunstein, J., Berdel, P., Gravius, S., Rohrbach, F., Oldenburg, J., Mayer, G., Potzsch, B., 2011. Profiling of active thrombin in human blood by supramolecular complexes. Angew. Chem. Int. Ed. Engl. 50 (27), 6075–6078.
Noiphung, J., Songjaroen, T., Dungchai, W., Henry, C.S., Chailapakul, O., Laiwattanapaisal, W., 2013. Electrochemical detection of glucose from whole blood using paper-based microfluidic devices. Anal. Chim. Acta 788, 39–45.
Oh, Y., Lee, H., Son, S.Y., Kim, S.J., Kim, P., 2016. Capillarity ion concentration polarization for spontaneous biomolecular preconcentration mechanism. Biomicrofluidics 10 (1), 014102.
Schaff, U.Y., Sommer, G.J., 2011. Whole blood immunoassay based on centrifugal bead sedimentation. Clin. Chem. 57 (5), 753–761.
Son, J.H., Lee, S.H., Hong, S., Park, S.M., Lee, J., Dickey, A.M., Lee, L.P., 2014. Hemolysis-free blood plasma separation. Lab Chip 14 (13), 2287–2292.
Song, Y., Huang, Y.Y., Liu, X., Zhang, X., Ferrari, M., Qin, L., 2014. Point-of-care technologies for molecular diagnostics using a drop of blood. Trends Biotechnol. 32 (3), 132–139.
Stroock, A.D., Dertinger, S.K., Ajdari, A., Mezic, I., Stone, H.A., Whitesides, G.M., 2002. Chaotic mixer for microchannels. Science 295 (5555), 647–651.
Truskey, G., Yuan, F., Katz, D., 2009. Transport Phenomena in Biological Systems. Pearson Education, New Jersey.
Tseng, C.-C., Yang, R.-J., Ju, W.-J., Fu, L.-M., 2018. Microfluidic paper-based platform for whole blood creatinine detection. Chem. Eng. J. 348, 117–124.
Volik, S., Alcaide, M., Morin, R.D., Collins, C., 2016. Cell-free DNA (cfDNA): clinical significance and utility in cancer shaped by emerging technologies. Mol. Cancer Res. 14 (10), 898–908.
Wang, J., Ahmad, H., Ma, C., Shi, Q., Vermesh, O., Vermesh, U., Heath, J., 2010. A self-powered, one-step chip for rapid, quantitative and multiplexed detection of proteins from pinpricks of whole blood. Lab Chip 10 (22), 3157–3162.
Weiner, J., Maertzdorf, J., Sutherland, J.S., Duffy, F.J., Thompson, E., Suliman, S., McEwen, G., Thiel, B., Parida, S.K., Zyla, J., Hanekom, W.A., Mohney, R.P., Boom, W.H., Mayanja-Kizza, H., Howe, R., Dockrell, H.M., Ottenhoff, T.H.M., Scriba, T.J., Zak, D.E., Walzl, G., Kaufmann, S.H.E., Consortium, G.C., 2018. Metabolite changes in blood predict the onset of tuberculosis. Nat. Commun. 9 (1), 5208.
Xu, L., Lee, H., Jetta, D., Oh, K.W., 2015. Vacuum-driven power-free microfluidics utilizing the gas solubility or permeability of polydimethylsiloxane (PDMS). Lab Chip 15 (20), 3962–3979.
Yan, S., Zhang, J., Chen, H., Alici, G., Du, H., Zhu, Y., Li, W., 2014. Making a hydrophoretic focuser tunable using a diaphragm. Biomicrofluidics 8 (6), 064115.
Yang, X., Forouzan, O., Brown, T.P., Shevkoplyas, S.S., 2012. Integrated separation of blood plasma from whole blood for microfluidic paper-based analytical devices. Lab Chip 12 (2), 274–280.
Yeh, E.C., Fu, C.C., Hu, L., Thakur, R., Feng, J., Lee, L.P., 2017. Self-powered integrated microfluidic point-of-care low-cost enabling (SIMPLE) chip. Sci. Adv. 3 (3), e1501645.